# Fatigue Analysis of the Effects of Wheel Load on Rail Life

R. K. STEELE AND M. W. JOERMS

**To obtain a proper assessment of wheel-load effects on rail fatigue life, both crack initiation and growth behavior must be considered. In order to do this, a small-crack growth model has been added to the three-dimensional initiation model PHOENIX. The combined model appears to make reasonable predictions in general agreement with observations from the Facility for Accelerated Service Testing (FAST). Exercise of the model suggests that modest increases in wear rate tend to lengthen crack initiation life but slightly shorten crack growth life. Total fatigue life (to 20 percent transverse defect) has been found to be approximately proportional to wheel load raised to the power of –2. If strong tensile stresses exist in the rail, fatigue life can be shortened greatly. However, the wheel-load dependency would be reduced somewhat (power of –1.5). The ramifications of introducing many heavier wheel loads are expected to be (a) a higher ratio of service failures to detected defects due to more rapid crack growth and (b) a larger number of detected defects. The ensuing loss of rail integrity can be balanced by taking a number of steps, including utilizing premium rail metallurgies with a more conformal contact profile, programming grinding to simulate wear, and adopting a rail performance approach to nondestructive inspection. In this approach actual detected defect and service failure experience acts to control inspection strategy.**

The continuing thrust of railroad operations toward heavier wheel loads calls into question the ability of rail to resist the heavier loads. A proper understanding of the effects of heavier wheel loads on rail performance cannot be obtained without consideration of other factors such as wheel-rail profile, improved strength and cleanliness of rail steel, and wear, that is, grinding.

The fatigue defect [shell/transverse defect (TD)], which forms internally within the rail head under the influence of the contact and residual stresses, is particularly amenable to fatigue analysis. Furthermore, some reliable experimental data (*1*) are available by which to gauge the correctness of a fatigue analysis. For these reasons and because the shell/TD has a high likelihood of causing a service failure with appreciable derailment potential (*2*), this paper will focus on that defect system.

As in all fatigue analyses, some caution must be exercised in defining fatigue life. Fatigue failures are characterized by a life distribution rather than by a single "life." Thus, the percentile of the population failed must be specified when life is calculated. Also, because of uncertainties about actual environmental conditions (i.e., loading, support, material), the fatigue analysis is more suited to illustrating expected trends in behavior than providing exact life estimates.

Association of American Railroads Technical Center, 3140 South Federal Street, Chicago, Ill. 60616.

## BACKGROUND

Fatigue fractures are frequently viewed as involving two processes: (a) initiation and (b) growth. During the initiation phase, the material is considered to remain "sound" (without a recognizable crack) until a crack opens within some small microstructural entity such as an individual metal grain. Growth processes then enlarge the crack, eventually to the point at which structural failure may occur.

The development of fatigue cracks in rail under the influence of wheel and rail contact stresses has been modeled by Chipperfield and Blickblau (*3*), Leis and Rice (*4*), Zarembski (*5*), and Lieurade et al. (*6*), among others.

The approach utilized by Chipperfield and Blickblau is based on opening and shear mode linear elastic fracture mechanics. They do not incorporate into their calculation those residual stresses that can exist within the rail. Their analysis predicts that a shell will initiate at approximately one-half the depth at which shells actually develop (i.e., 1/4 to 3/8 in.). The analysis does, however, predict the correct size for the shell (10 mm) when the TD first appears. However, they do not address the issue of why some shells do not turn into TDs.

The analyses of Leis and Rice and of Lieurade et al. are based on calculations of equivalent strain range determined from three-dimensional stresses, including the service-induced residual stresses. Neither analysis appears to treat growth of the shell or development of the TD. Both appear to predict shell occurrence at approximately the correct depth.

Even though the analyses appear to be similar in nature, each suggests a very different estimate of wheel-load dependence. The Leis-Rice analysis suggests that a 50 percent increase in wheel load will produce about a 50 percent decrease in life when measured in million gross tons (MGT), with no residual stresses considered or about a 23 percent decrease in life if observed service-induced residual stresses are included. On the other hand, Lieurade et al. state that "service life can be reduced by a factor of 1,000 when $p_0/k$ (contact stress/yield strength) changes from 4.5 to 6, a 33 percent increase in contact stress. Usually Hertzian contact stress is proportional to wheel load raised to about the one-third power (*7*), so a 33 percent increase in pressure is approximately the equivalent of a 135 percent increase in wheel load. It is not clear whether the factor of 1,000 applies to cycles of loading or to MGT as the units of service exposure. On the basis of very limited revenue service data from sites that are not necessarily equivalent (*1*), the Leis-Rice estimate appears somewhat low and the Lieurade et al. estimate, very high.

Rather interestingly, the approach used by Zarembski also predicts a high dependency of rail life on wheel load, similar

in fact to that reported by Lieurade et al. However, the Zarembski method uses only uniaxial stresses and ignores the three-dimensional nature of contact stress. Furthermore, it does not incorporate the service-induced residual stresses, and therefore predicts maximum fatigue damage to occur at the rail head running surface rather than internally, where shells are actually observed to form.

Yet the computational approach used by Zarembski is simple in concept and straightforward in operation, which allows high computational efficiency. Thus, over the course of the last 4 years, both the Association of American Railroads (AAR) and the Transportation Systems Center (TSC) of the U.S. Department of Transportation have modified this approach to incorporate three-dimensional stresses, including service-induced residual stresses. Perlman et al. and Steele have described the results of exercising both versions of the model. The AAR version is called PHOENIX; its computational approach is described in the appendix.

## FATIGUE MODEL

PHOENIX is primarily a crack initiation model that uses the following stress systems:

1. Contact stresses calculated for Hertzian contact without the presence of surface tractions;
2. Three-dimensional residual stresses, specifically those found experimentally by Schilling and Blake (*10*) to be typical [similar residual stress distributions, reported by Groom (*11*), are shown in Figure 1];
3. Uniaxial beam bending stresses and head-on-web (HOW) bending stresses (*12*); and
4. Uniaxial stresses caused by the deviation of the rail temperature from the neutral temperature or by rail creep.

The basic rail steel fatigue characteristics are those reported by Fowler (*13*) in the form of constant stress amplitude or life (i.e., *S/N*) data. The fact that many tests were run at each stress amplitude level allows an estimation of the *S/N* relationships at a number of life percentiles. The reaggregation of all of Fowler's longitudinal *S/N* data is shown in Figure 2.

The rail surface region becomes work hardened under repeated action of passing wheels, which also improves fatigue resistance (*14*). The model has been modified to accept the variation of hardness from the running surface inward and to pick appropriate fatigue (*S/N*) characteristics to use at each level of hardness.

Wear (or grinding) can be simulated by the computational removal of surface material while the work-hardening and residual-stress gradients remain fixed with respect to the current surface. This simulation is valid when the rate of wear is small compared with the rate at which the surface work-hardens. Typically this is done incrementally at 10-MGT intervals during damage calculation.

PHOENIX calculates the service exposure in MGT to produce the very first manifestation of a fatigue crack (shell) beneath the running surface of the rail. This first manifestation would not be observable, however, except by fortuitous destructive sectioning right at the point of initiation. At the stress levels at which initiation is calculated to occur, the life to

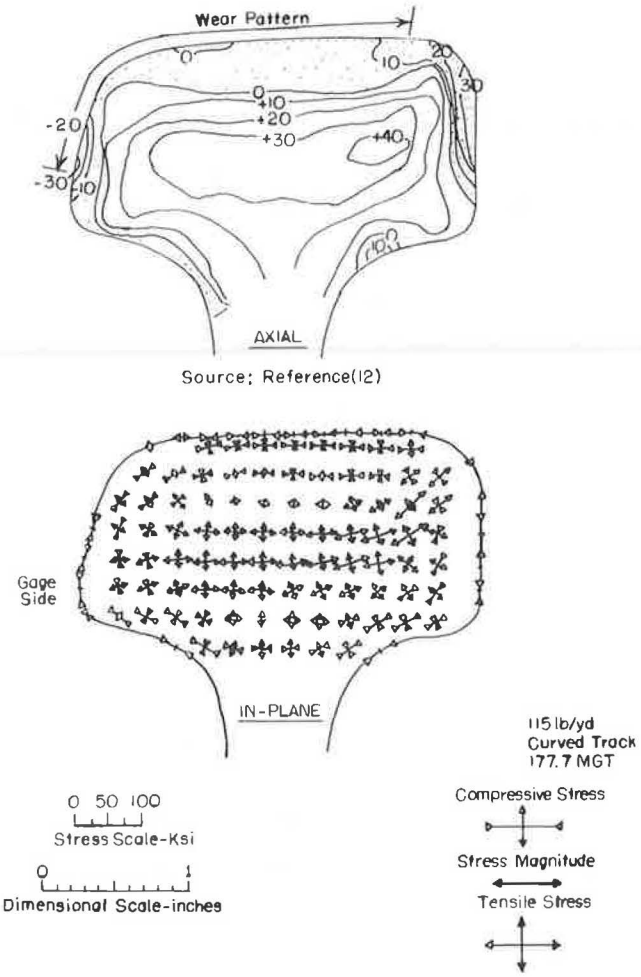


**FIGURE 1 Axial and in-plane residual stresses in a service-worn rail (*12*).**

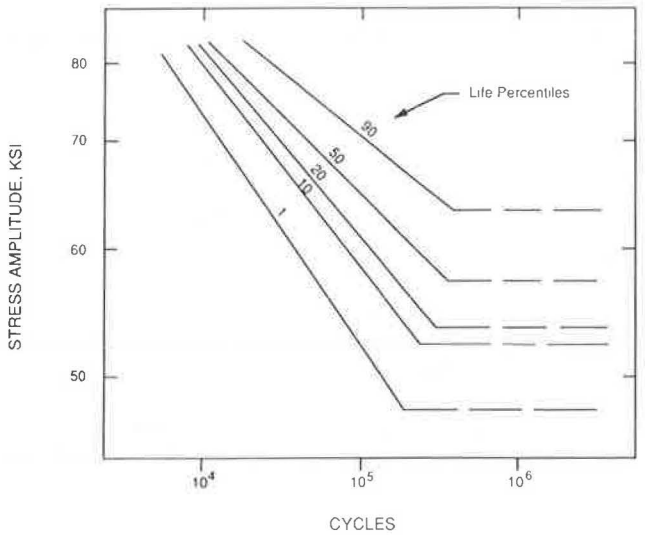


**FIGURE 2 Reaggregated *S/N* data for standard carbon rail.**

macroscopic crack initiation would be expected (*15*) to be a large part (perhaps 90 to 95 percent) of total life. Thus initiation life alone may, in most cases, be adequate for engineering estimates.

However, when an estimate of structural integrity is sought, some knowledge of the likelihood of finding the defect must enter into consideration. Because the ability to find a defect nondestructively depends on the size of the defect, the growth behavior needs to be established.

The growth of the shell and its subsequent turning into a TD have been treated analytically by Hearle and Johnson (*16*) and by Farris et al. (*17, 18*). However, the rigorous computation is far too complex to be incorporated into PHOENIX at this time. Thus, a simpler, interim modeling approach treating TD growth alone has been developed, which is compared in Figure 3 with actual growth. This approach makes the tacit

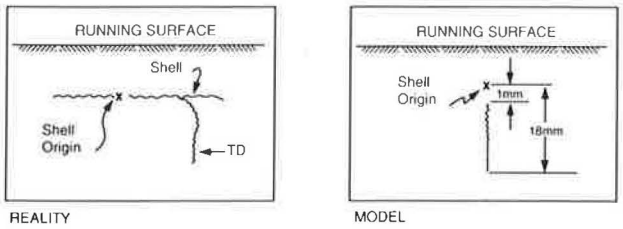


**FIGURE 3 TD growth from shell versus modeled growth.**

assumption that the period of shell growth before the development of a TD (1 mm in radius) is small compared with the total service exposure life and can be neglected in making engineering judgments.

Following from the work of Orringer et al. (*19*), the growth relationship has been taken as

$$da/dN = C\,\Delta K_{\text{eff}}^{n}/(1 - R) \tag{1}$$

where

$da/dN$ = crack growth rate,
$a$ = crack radius,
$N$ = cycles of loading,
$C$ = $10^{-11}$ in./cycle,
$R$ = stress ratio (minimum stress divided by maximum stress),
$n$ = slope of logarithmic plot of $da/dN$ versus $\Delta K$, and
$\Delta K_{\text{eff}}^{n}$ = effective stress intensity range,

$$\Delta K_{\text{eff}}^{n} = (\Delta K_{\text{I}}^{2} + \Delta K_{\text{II}}^{2})^{1/2} \tag{2}$$

where the subscripts I and II refer to the crack opening and vertical shear modes, respectively. The incorporation of a shear contribution into the growth analysis was necessary because early trials of the growth model using only the opening mode stress intensity revealed growth periods far longer than observed to be reasonable. The limitations of blending opening and shear modes, specifically as shown in Equation 2, have been discussed by Besuner (*20*).

In the analysis, the TD is treated as a penny-shaped crack embedded in an infinite solid so that the relationship between stress intensity and stress and crack radius is simply

$$\Delta K_{\text{eff}} = 1.13\Delta\sigma_{\text{eff}}(a)^{1/2} \tag{3}$$

Strictly speaking, Equation 3 is not the correct formulation, because the transverse crack does not grow in a self-similar fashion, that is, retaining its circular shape, by the same radial growth from its origin in all directions. The non-self-similar growth behavior is shown in Figure 4 (*21*). This asymmetry of growth results from the difference between the steady (residual) stresses above the defect origin (compression) and those below it (tension). Nevertheless, the lower portion of the crack front remains approximately circular and is centered on the TD origin (at the shell) for crack sizes up to approximately 10 to 15 percent of the rail head cross-sectional area. However,

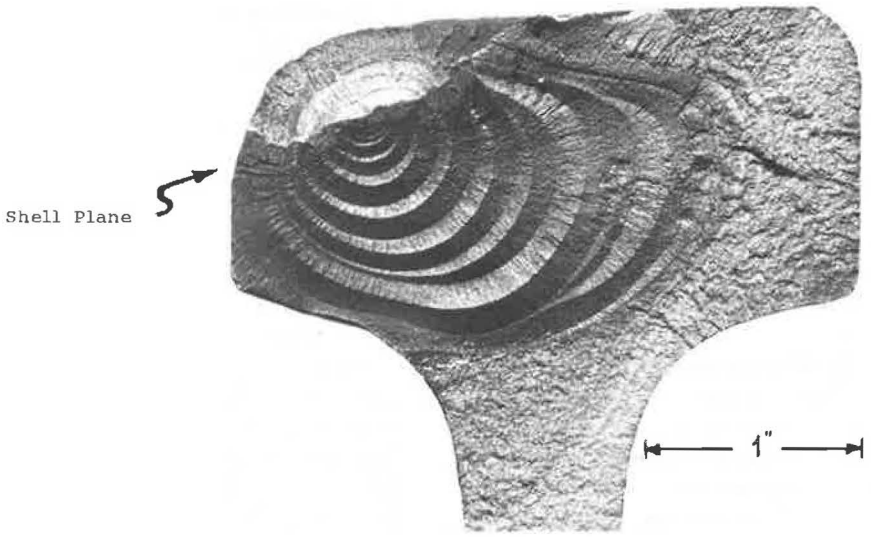


**FIGURE 4 TD originating from a shell, showing progressive growth rings.**

the area of the TD is generally about 60 percent that of a circle whose radius extends from the TD origin to the lower crack front.

The Mode I live (varying) stresses result from beam bending, HOW bending, temperature variation, and downgrade rail creep (caused by train braking and tractive effort in climbing grades) along the track. Beam bending is calculated for a rail supported on a continuous foundation such that as a wheel passes, the rail head at a specific point will experience about five times the stress in compression than the maximum that will occur in tension (reverse bending). Maximum reverse bending occurs when the wheel is approximately 5 ft from the point of maximum compression flexural stress. The HOW stresses are calculated for the rail head acting as an independent beam supported continuously by the web of the rail. They are superimposed on the beam-bending stresses, tending to produce a tension peak at the bottom of the rail head when the wheel is directly above (Figure 5). Their effect is most acute when the track structure is stiff.

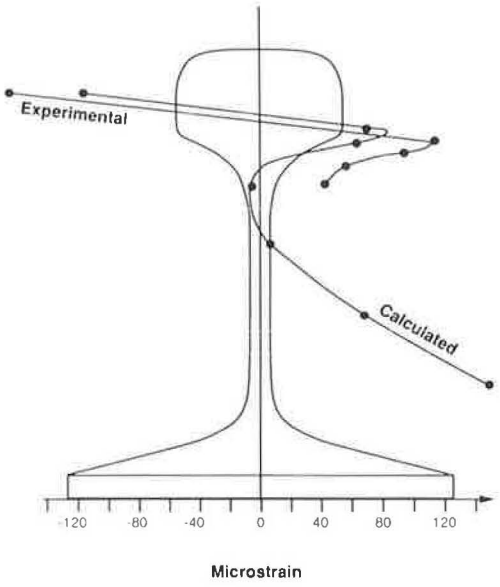


**FIGURE 5 Head-on-web bending strains for rail on stiff track.**

The Mode II stresses result from beam shear (maximum at the neutral axis of the rail), HOW shear (maximum approximately at the mid-height of the rail head), and contact shear, which reaches its maximum, in the absence of surface tractions, approximately 0.1 to 0.15 in. beneath the surface. In calculation of the HOW shear, the head is treated as a beam supported across its entire width when in reality it is supported only over the central third of its width. Thus, the HOW shear stress contribution may be overemphasized. The relationship of the bending-induced shears is shown in Figure 6. Interestingly, below the depth of maximum contact shear (0.1 to 0.15 in.), the contact shear amplitude is approximately 27 percent of the vertical (compression) stress at each point (*7*). This relationship has been used to simplify the calculation. All shear stresses are treated as being fully reversed and are added algebraically together.

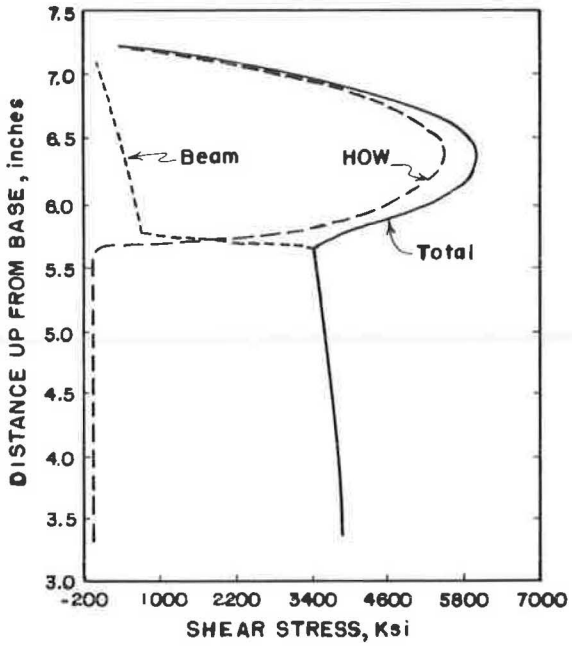


**FIGURE 6 Beam and HOW shear stress distribution.**

The calculation of the growth curve proceeds incrementally from the integrated form of Equation 1, that is,

$$a_f = a_i/[a_i C'(1.13\Delta\sigma_{eff})^n \Delta N + 1] \quad (4)$$

where

$C'$ = $C/(1 - R)$;
$a_i, a_f$ = crack radii at the beginning and end of interval $\Delta N$, respectively; and
$\Delta N$ = number of cycles of loading for each block of the load spectra.

As the crack grows into regions of different stress, the level of stress is adjusted to be that calculated to exist at the position of the crack tip as if no crack actually existed there.

The crack growth characteristics of rail steel are taken to be those described by Scutti (*22*); they are shown in Figure 7. Although the typical slope $n$ of the data trend is near 4, some variation is apparent.

## RESULTS

Before a look at the combined effects of shell initiation and transverse crack growth, the predictions of the crack growth model need to be examined for agreement with observed crack growth behavior. Regrettably, the only known growth information for small TDs (from a few percent up to 10 to 15 percent) is that reported (*1*) for a defect in a 4-degree curve at the Facility for Accelerated Service Testing (FAST). Failure of the rail occurred late in a rather cold February, suggesting the presence of thermal tension stress.

To model this behavior, the following conditions have been specified as inputs into both the initiation and growth parts of

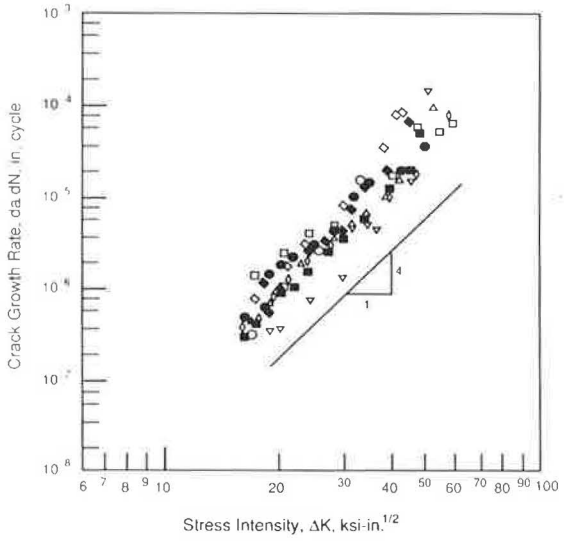


**FIGURE 7 Crack growth behavior of rail steel (*22*).**

the model (the initiation model is used to locate the depth of the origin of the TD):

Rail section: 115 lb/yd;
Track stiffness μ: 5,000 psi;
Wheel load (average): 32.2 kips [32.2 kips is the vectorial sum of the typical average FAST wheel load (30.3 kips) and a typical lateral load (11 kips)];
Load spectra: FAST type;
Wheel diameter: 36 in.;
Rail crown radius: 5 in., 20 in.;
*S/N* characteristics: reaggregated;
Life percentile: 5th;
Residual stresses: standard (Figure 8);
Thermal stresses: 0, +15 ksi.

Before examination of the results of the parametric exercise, a few words are necessary about the variation in rail crown radius. When wheels run on rail in tangent track, the contact zone on new rail is generally near the center of the rail head, just slightly to the gage side. At that position the worn rail crown radius is about 20 in. (*23*). However, when the rail is in a curve, the wheel "footprint" extends all the way from the gage face to about one-half the distance from the center to the field side of the rail head (Figure 9). Thus, it is not clear what crown radius should be used in the analysis. Over the shell defect, the radius of curvature of the worn rail varies continuously from less than an inch to about 20 in. near the center of the rail head (Figure 10).

Nor is it clear how much of the vertical wheel load is partitioned from the ball of the rail to the gage face. Curving model analysis (*23*) for the FAST worn-wheel and worn-rail profiles suggests that under unlubricated conditions nearly 50 percent of the vertical load can be carried on the gage face. Under lubricated conditions, this is calculated to drop to about 35 percent. This pattern is shown in Figure 11.

Yet another concern is that PHOENIX makes the contact stress calculation for the crossed cylinder contact configuration (wheel profile radius = ∞). However, the worn wheel rolling on the worn rail represents a more conformal situation. For this case, the wheel profile radius at the point of contact typically is not infinity but more nearly about 5 in. greater than the rail profile radius at that point (*24, 25*). Thus, a large number of different wheel and rail profile contact arrangements could produce the same contact stress. This is shown in Figure 12, which has been prepared from the work of Kumar and Singh (*26*) for a 36-in. diameter wheel. Here a 5-in. rail profile crown radius in contact with a 10-in. wheel profile radius yields a contact stress of about 200 ksi (33-kip wheel load). The same contact stress could be achieved with an approximately 9-in. rail crown radius in contact with a 35-in. wheel profile radius. The equivalent crossed cylinder configuration would have a 12-in. rail crown radius.

In recognition of all these uncertainties, the contact situation for curving (with flanging) has been treated by including both the 5- and the 20-in. rail crown radii in the calculations. The results of these calculations are shown in Figures 13 and 14.

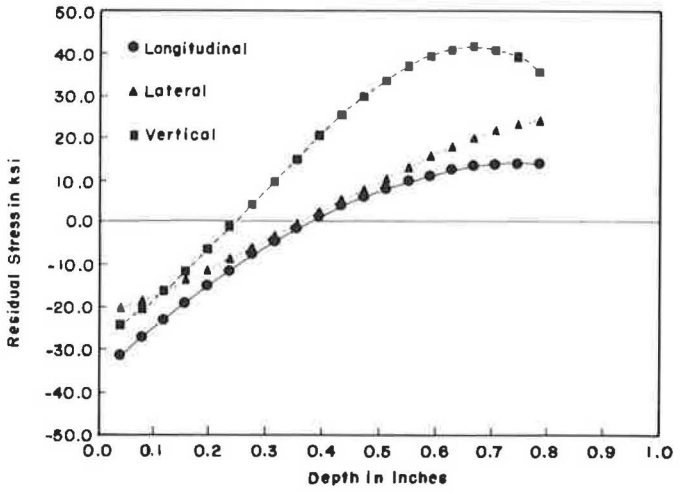


**FIGURE 8 Residual stress profiles used in PHOENIX.**

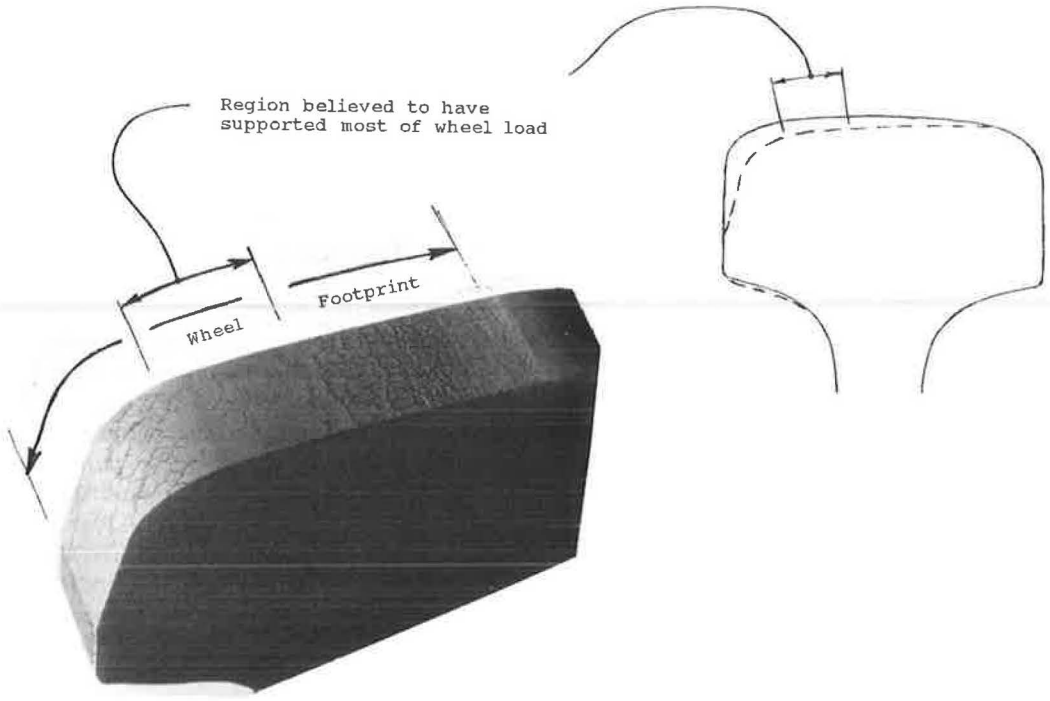


**FIGURE 9 FAST failed rail (4-degree curve/gage face and tread).**

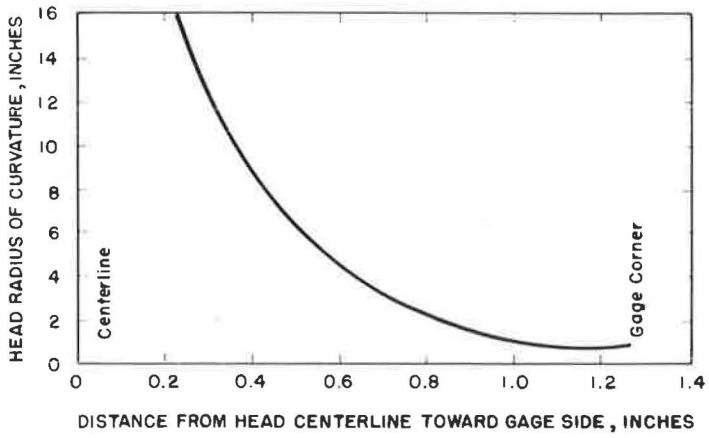


**FIGURE 10 Variation of FAST worn rail crown radius of curvature across gage side half of rail head.**

With all shear stress contributions included and no thermal stress, both the 5- and the 20-in. rail crown radii lead to significantly shorter predicted crack growth lives than that actually observed. However, if the model were to overemphasize the contribution of the HOW shear, the two different crown radii would cause the life prediction to bracket the observed behavior; that is, with the 5-in. (crossed cylinder) crown radius, the model predicts too short a life, whereas with the 20-in. (crossed cylinder) crown radius, the model predicts too long a life.

With the +15-ksi static stress included to represent the likelihood that a thermal stress would occur in February, the predicted growth behavior for the 20-in. crown radius (with no load partitioning) is much closer to that observed. The thermal stress does not have much of an effect until the defect radius reaches 5 mm (20-in. crown radius) and 10 mm (5-in. crown radius).

The initiation life and initiation depth also yield some clues about the appropriateness of the predictions. As can be seen in Figure 4, the depth of initiation was about 0.35 in. and the total service exposure had been estimated to be about 180 MGT (*1*). Remarkably, the 20-in. crown radius without HOW shear but with a +15-ksi tensile thermal stress leads to an initiation-life prediction of 174 MGT (total life ≈ 220 MGT) and a depth of initiation of 0.32 in.—which is not very far from what was actually observed.

The same contact stress calculated to exist with a 20-in. crown radius (crossed cylinders) could also result from an 8-in. crown radius in conformal contact with a 14-in. wheel profile radius (Figure 12). The wear pattern and the head

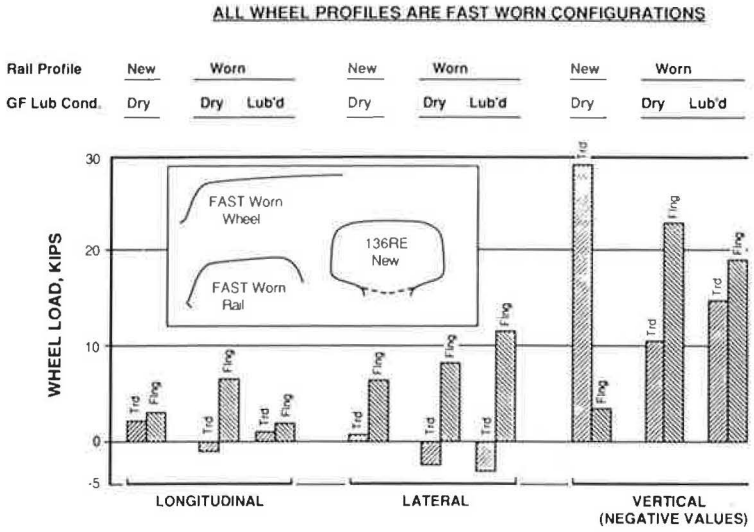


**FIGURE 11 Effect of flange contact and lubrication state on wheel force distribution on high rail of curve.**

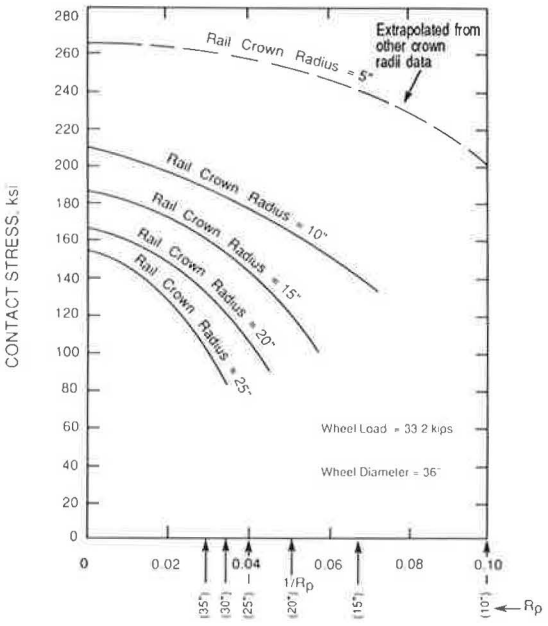


**FIGURE 12 Variation of contact stress with reciprocal of wheel profile radius.**

check-free zone about 1/2 in. toward the gage face from the rail head center (Figure 9) do suggest that this location was the predominant wheel loading path. At that point, Figure 10 indicates that the rail crown radius should be near 6 to 7 in.

There remain uncertainties about (a) the actual load on that path (how much is partitioned to the gage face), (b) the wheel profile radius at contact, (c) the thermal stress level imposed during initiation and growth, and (d) the actual fatigue characteristics of the failed rail. Thus, in the remainder of the analysis to be described here, the HOW shears will be included to provide a conservative estimate of crack growth behavior.

Figures 15 and 16 show the effect of track stiffness on crack growth for a heavier rail section (136 lb/yd), again with the components of shear stress turned off one at a time. When the TD is small, the contact shear stresses have the dominant effect. With all shear stresses operative, reducing the track stiffness by a factor of 5 shortens the crack growth life at any specified crack size by a factor of about 2.

The FAST Defect Initiation and Growth Experiment results can also serve as a basis for checking the validity of the crack growth calculations. Orringer et al. (*19*) have reported the FAST growth behavior of a number of TDs transplanted from revenue service into FAST tangent track. At small defect sizes in the range of 10 to 20 percent, the area growth behavior appears to be linear, ranging from a low near 0.25 percent/MGT to a high near 1.3 percent/MGT. (A linear relationship of defect area with MGT implies that for a circular defect, the rate of crack front movement decreases with increasing MGT as the defect becomes larger.) These 0.25- and 1.3-percent slopes (converted to radial growth) are shown in Figure 16 at 11 percent defect size. They are arbitrarily positioned at 45 MGT to allow slope comparisons. The steeper of the two slopes is very close to the slope of the calculated growth curve, where contact and HOW shears at least are operative. This encourages belief that the transverse crack growth computation method is appropriate.

Lest one become too confident of that, though, a significant caveat must be noted: transverse crack growth behavior can depend strongly on where the crack initiation part of the model positions the "center" of the TD. Figure 17 shows what can happen if the ultimate tensile strength used in the initiation calculation is too low. Specifically, increased wheel load can be calculated to initiate a shell at much greater depth (a different position in the residual stress field) so that the crack growth is actually less rapid. When initiation occurs at the same (or only slightly different) depth, the heavier wheel loads increase the rate of crack growth, shortening the growth period by about 35 percent for the 18 percent increase in wheel load from 33 to 39 kips.

Crack growth behavior is extremely sensitive to the value of the power term $n$ (Equation 1). Although the typical value

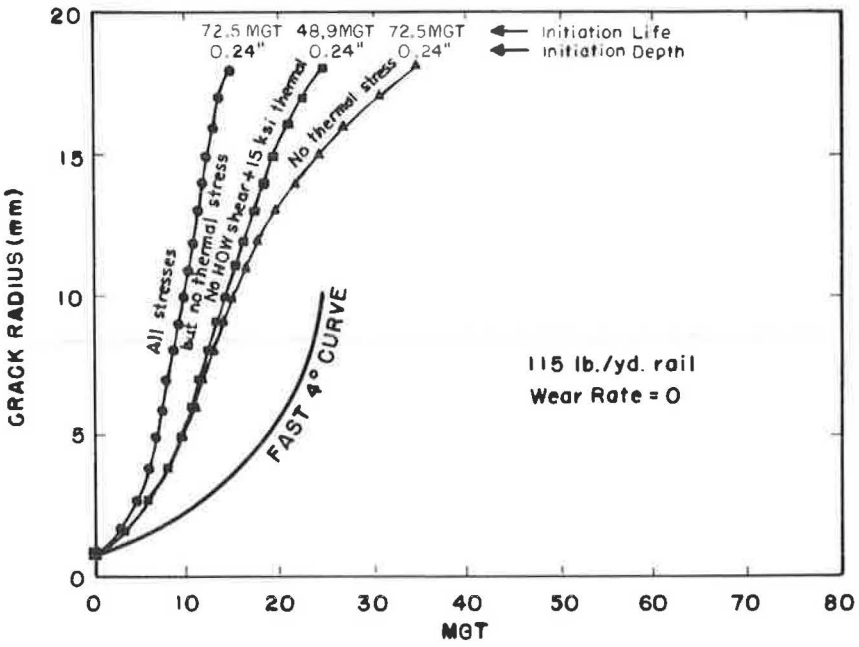


**FIGURE 13 Comparison of predicted and observed transverse crack growth behavior (5-in. crown radius).**

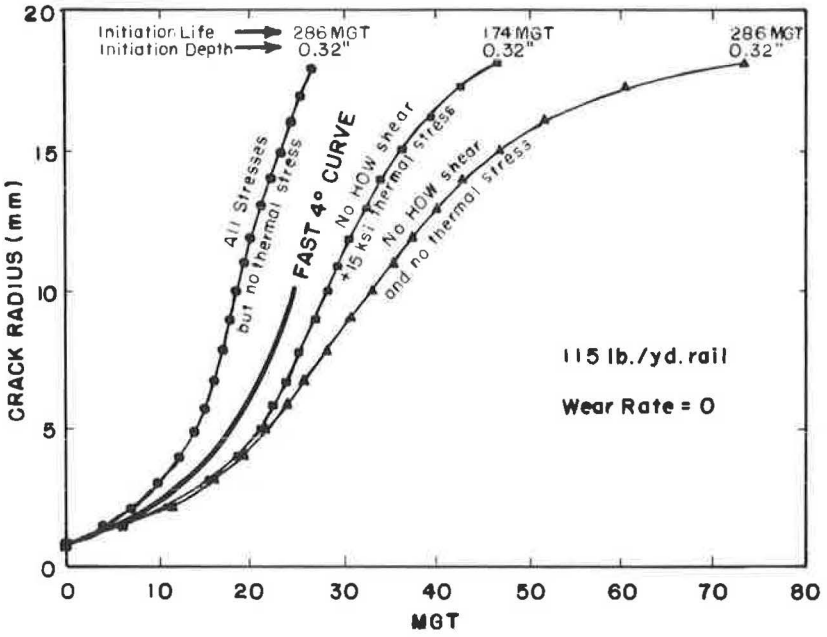


**FIGURE 14 Comparison of predicted and observed transverse crack growth behavior (20-in. crown radius).**

appears to be near 4 (Figure 7), some variation does occur. Figure 18 shows the very large variation in crack growth behavior that would be expected for relatively small variations in the value of *n*.

The last two paragraphs have exemplified how much the modeler of fatigue processes is at the mercy of his uncertainty of material properties as well as of environmental characteristics.

With these caveats in mind, initiation and growth can be combined to examine quantitatively the trends to be expected from variations in wheel load. Because most revenue service track is less stiff than that at FAST, and to simulate a realistic support environment leading to relatively rapid crack growth, a track stiffness of 1,000 psi was selected. The life predictions (both initiation and total life to 20 percent TD size) are shown as a function of wear rate in Figure 19. The service lives calculated here are based on a common residual stress pattern (Figure 8) for all three wheel loads. In fact, that pattern and magnitude of stresses would be a function of wheel load. A rail subjected to only 19-kip wheel loads would be expected to

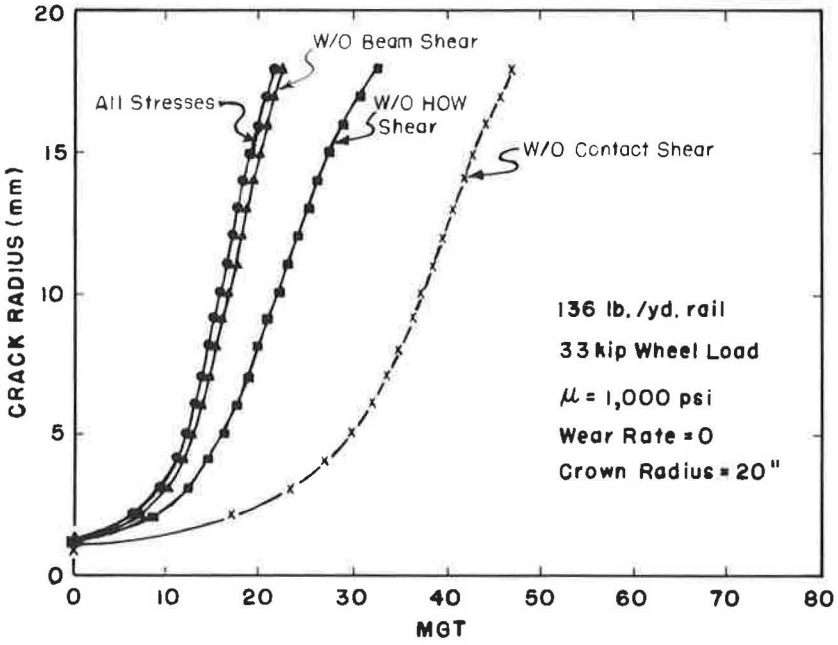


**FIGURE 15 Contribution of different shear stress systems to growth behavior: μ = 1,000 psi.**

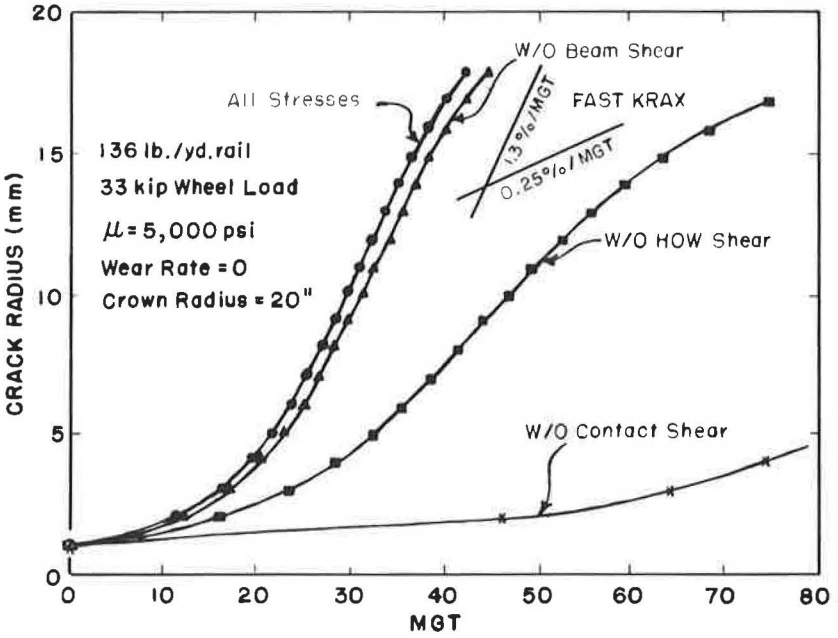


**FIGURE 16 Contribution of different shear stress systems to growth behavior: μ = 5,000 psi.**

exhibit less plastic flow and therefore lower residual stress levels with a less well-developed pattern. A rail exposed to only 39-kip wheel loads would be expected to have a somewhat more pronounced residual stress pattern than that used in the analysis as well as somewhat higher stress levels.

Increasing the wear rate is calculated to have two effects. It tends to lengthen the initiation life; a flatter (larger-radius) rail crown curvature tends to enhance the life benefit of an increased wear rate (*9*). However, it tends to shorten the growth life. The effects of the wear rate are more noticeable at the lower wheel loads. Overall, the effect of increasing the wear rate is to increase the total life. Considering initiation of the shell alone, the effect of the wear rate on life is predicted to be even more pronounced with higher-strength rail. This is shown in Figure 20, which also shows that fatigue life improvement attributable to the use of a high-premium rail will be expected to be about a factor of 2 at zero wear rate. However, it will be closer to a factor of 2.5 at a wear rate near 1.6 mm/100 MGT.

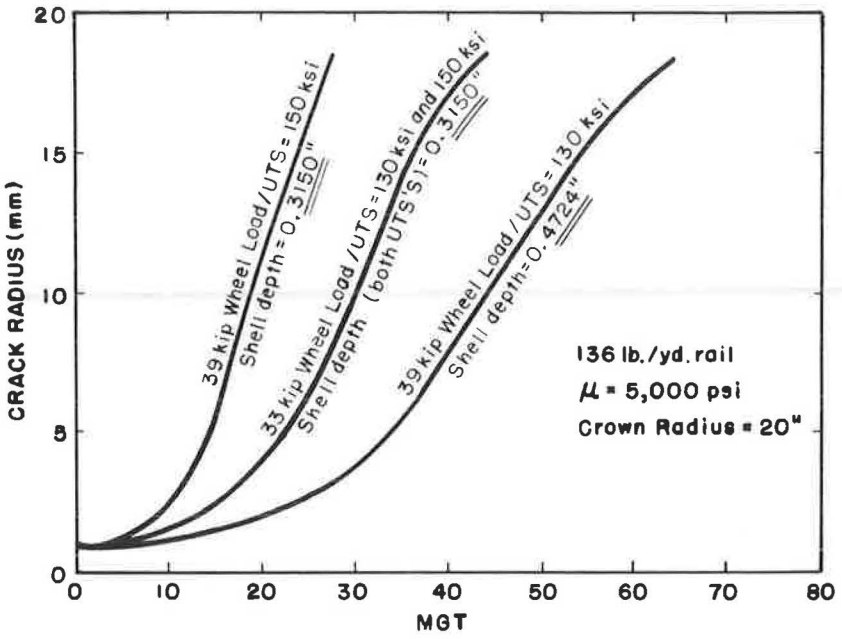


**FIGURE 17 Effect of ultimate tensile strength on calculation of crack growth behavior.**

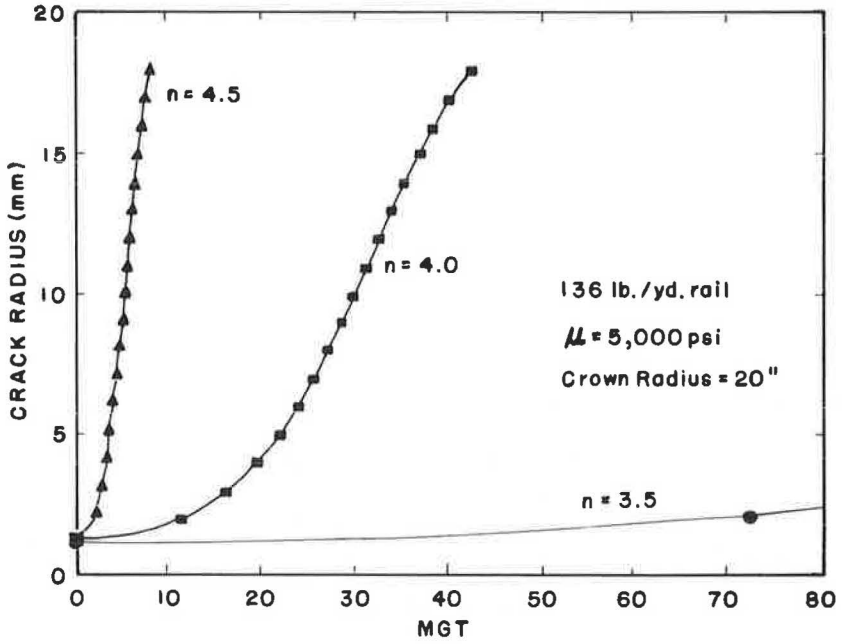


**FIGURE 18 Effect of crack growth exponent on crack growth behavior.**

The wheel-load dependence may be seen more clearly if the data are plotted as shown in Figure 21. Here the total life to 20 percent TD size is given for both the standard residual stress case and for the case in which a 15-ksi steady tension stress has been imposed along the rail. The latter situation can develop during a cold period or from the creep of rail down a grade. A revenue service typical wear rate of 1 mm/100 MGT was used in the calculation. In both cases, the following relationship applies:

$$\text{Service life (5th percentile, MGT)} \propto (\text{wheel load})^m \quad (5)$$

where $m$ is $-2$ for the standard case. The 15-ksi tension has reduced expected service life significantly (about 50 percent). It also has reduced the value of $m$ to $-1.5$, that is, it has decreased the wheel-load dependence somewhat.

## DISCUSSION

The combined initiation-and-growth model used here appears to produce believable initiation-and-growth predictions, at least on a comparative if not an absolute basis. The wheel-load dependence predicted ($m = -1.5$ to $-2$) is in close agreement

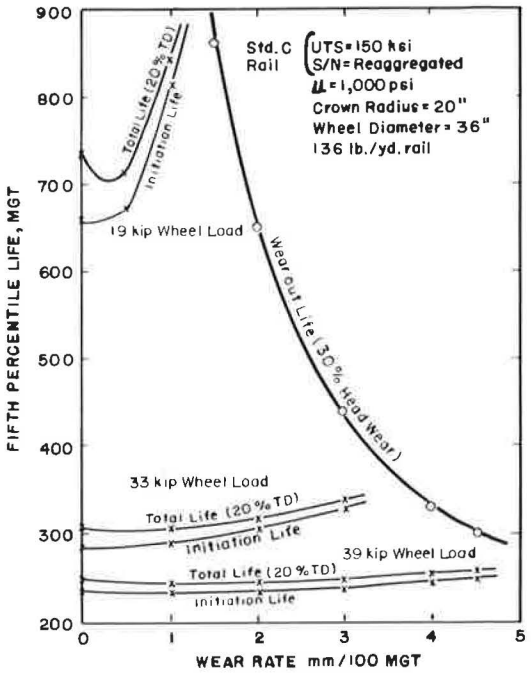


**FIGURE 19 Effect of wear rate on 5th-percentile fatigue life of standard carbon rail at different wheel loads.**

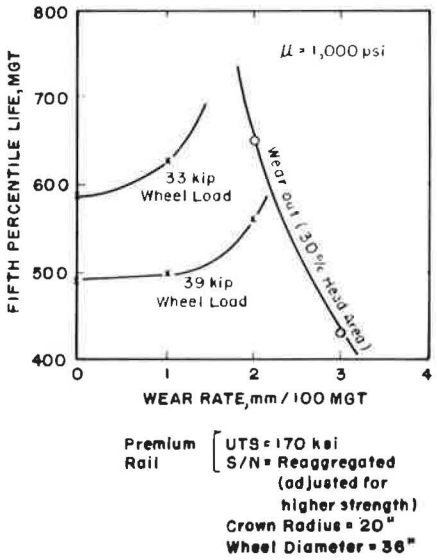


**FIGURE 20 Effect of wear rate on 5th-percentile initiation life of premium rail steel (320 BHN).**

with an analysis of revenue service rail failure behavior made by Steele and Reiff (*1*). Both of these predictions are then in closer agreement with the predictions of Leis and Rice (*4*) than with the calculations of Zarembski (*5*) and of Lieurade et al. (*6*).

However, before the reader becomes too convinced of infallibility, he should be aware that the model also makes some other predictions that may or may not be reasonable. Specifically, the initiation model interprets compression acting along the rail as beneficial in prolonging shell initiation life. Thus,

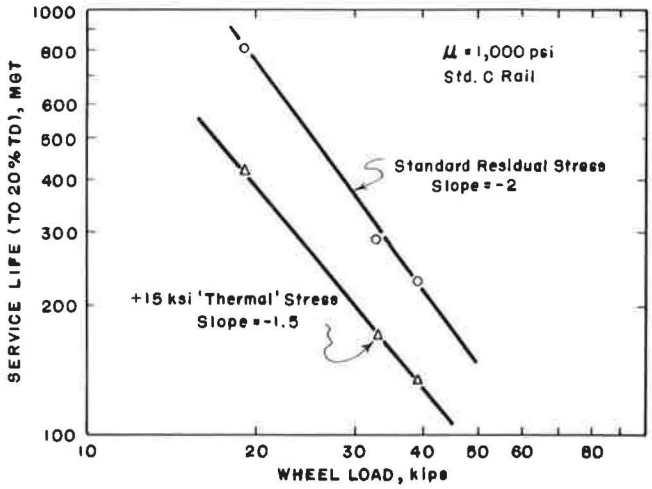


**FIGURE 21 Service life as a function of wheel load with and without additional "thermal" stress component.**

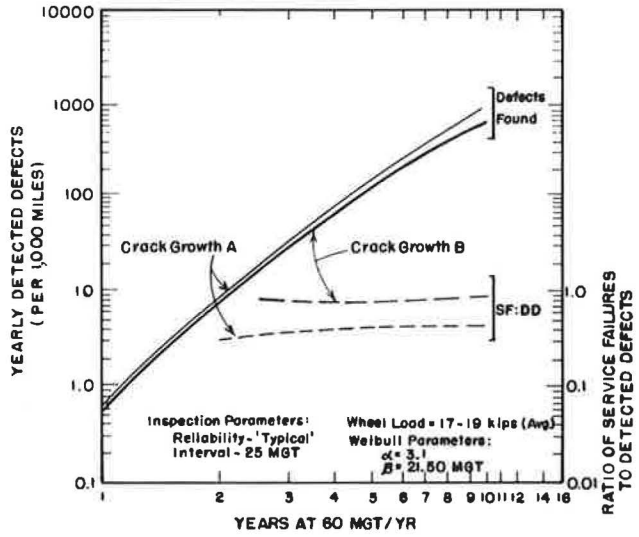


**FIGURE 22 Variation of detected defects and ratio of service failures to detected defects with service exposure for two different crack growth behaviors.**

soft track and light rail sections are calculated to have slightly longer initiation lives, with all other parameters (especially crown radius) kept constant. There are some field defect data (*1*), the exact wheel loadings and wear rates for which are not really known, that suggest that lighter rail sections have poorer rail head defect fatigue service lives. However, there are also published rolling load test data (27) to suggest that the level of flexural stress (and by inference rail section and track stiffness) has little effect on shell initiation.

The ramifications of the projections of decreased rail fatigue life made in this paper for heavier wheel loads will be felt most keenly in the increased likelihood of service failure occurrence. The relationship between rail failure behavior and rail integrity has been treated by Davis et al. (*28*). Specifically, the effects of increased crack growth rate and higher initiation rate have been considered, albeit separately. Were no other changes to occur, reducing the crack growth period by 50 percent would be expected to approximately double the ratio of

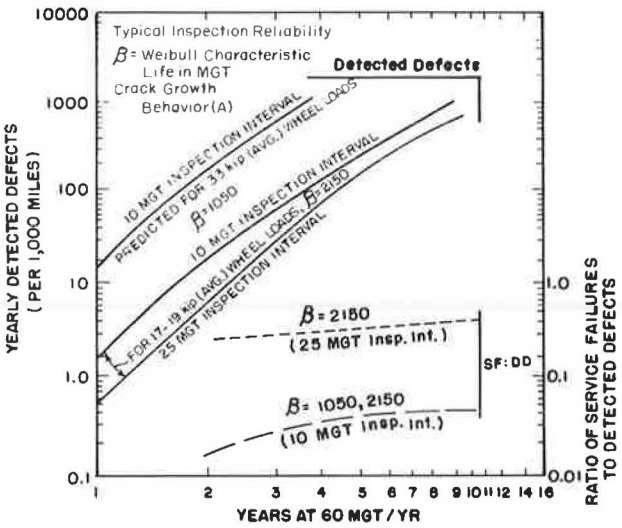


**FIGURE 23 Predicted effect of increased average wheel load on detected defects and ratio of service failures to detected defects.**

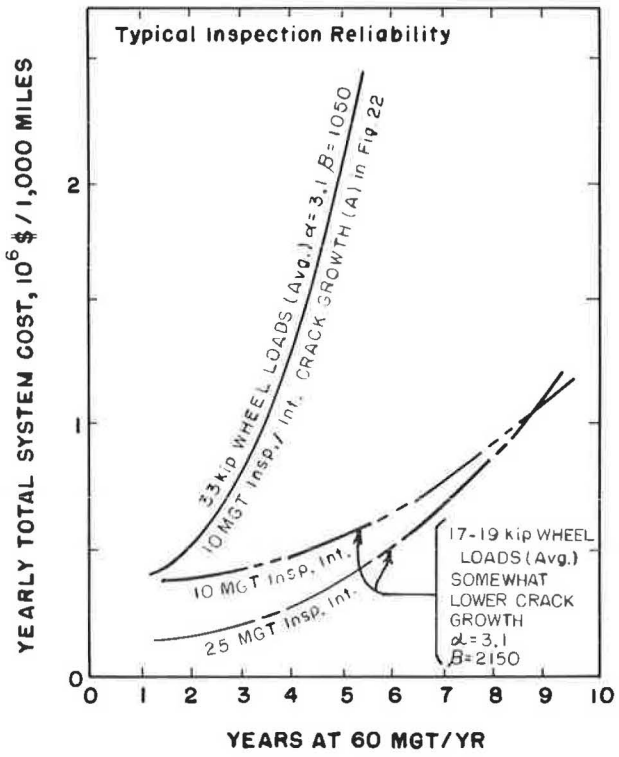


**FIGURE 24 Predicted effect of increasing average wheel load from 17 to 19 kips to 33 kips on yearly total system cost.**

service failures to detected defects. This is shown in Figure 22 for a 60-MGT/year line (17- to 19-kip wheel loads) with inspections at 25-MGT intervals. Changing from all 17- to 19-kip wheel loads to all 33-kip wheel loads (keeping crack growth behavior fixed) would not alter the ratio of service failures to detected defects (Figure 23) at a fixed inspection interval. But the number of detected defects would increase by a factor of 8 to 9 for a fixed inspection interval of 10 MGT.

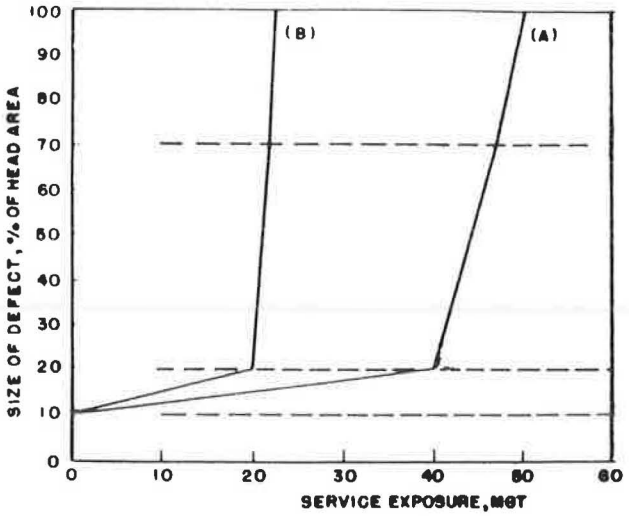


**FIGURE 25 Crack growth behavior used for 17- to 19-kip (B) and 33-kip (A) wheel loads.**

The cost analysis performed by Moore (*27*) did not include 39-kip wheel loads, but examination of the differences in costs between all 17- to 19-kip wheel loads and all 33-kip wheel loads is enlightening. Figure 24 gives the calculated yearly total system costs for 33- and 17- to 19-kip wheel loads. The crack growth behavior used for the 33-kip wheel loads was that shown by curve A in Figure 25. For 17- to 19-kip wheel loads, the crack growth rate used was somewhat slower, requiring 60 MGT instead of 45 MGT to reach 70 percent size. This is not as slow as the fatigue analysis in this paper suggests that it should be at the lower wheel loads. But the results are appropriate enough to illustrate the large cost penalties for an approximately 80 percent increase in wheel load.

Thus, the projections of this analysis and the analyses made by Moore (*27*) suggest that significant increases in yearly total system cost will occur with the introduction of large numbers of heavier wheel loads, unless changes are made in any or all of the following parameters:

- Rail metallurgy and running surface design,
- Rail maintenance practice (i.e., grinding), and
- Rail nondestructive inspection (NDI).

Improvements in rail metallurgy (rail with a Brinnell Hardness Number of 300) and rail head manufactured profile may be expected to provide very effective compensation for heavier wheel loads (*23*). But their introduction may be slow because of the substantial track mileage that would need to be replaced. In contrast, rail grinding and NDI are practices easily applied to in-track rail to preserve integrity. Grinding, which both reconfigures the rail contact surface and simulates wear, can alter the defect initiation Weibull parameters, especially increasing the characteristic life, 8. The use of a rail performance (i.e., rail integrity) guideline for rail defect inspection can achieve lower total system cost through improved management of existing inspection resources. As wheel loads increase and cause more rapid crack growth, more sensitive inspection techniques will offer significant cost advantage and will allow the same level of integrity to be achieved under more adverse conditions without increasing the number of rail inspections.

## SUMMARY

A means of performing transverse crack growth calculations (1- to 18-mm radius) has been incorporated into the three-dimensional fatigue initiation model PHOENIX. In order to reproduce observed crack growth rates at small defect size, the inclusion of a shear mode contribution to stress intensity has been necessary. The complete model has been exercised for conditions simulating the FAST environment, with results close to those actually observed experimentally. Projections made for revenue service conditions (softer track) suggest that the influence of wheel loads on fatigue life is dependent appreciably upon wear rate. Large tensile (thermal) stresses reduce expected life significantly (about 50 percent). Generally,

Service life (MGT) = (wheel load)$^m$

where $m$ is –1.5 to –2. Although heavier wheel loads can be expected to reduce rail fatigue life, the problem can be managed satisfactorily by improving rail metallurgy and design, rail repair practice, rail inspection strategy, or all three.


## REFERENCES


1. R. K. Steele and R. P. Reiff. Rail: Its Behavior and Relationship to Total System Wear. *Proceedings, Second International Heavy Haul Railway Conference*, Association of American Railroads et al., Sept. 1982, pp. 227–276.
2. R. K. Steele. Requirements for the Reliability Assessment of Railroad Rail in Service. *Railroad Track Mechanics and Technology*, 1978, pp. 303–322.
3. C. G. Chipperfield and A. S. Blickblau. Modeling Rolling Contact Fatigue in Rails. *Rail International*, Vol. 15, No. 1, 1984, pp. 25–31.
4. B. N. Leis and R. C. Rice. Rail Fatigue Resistance—Increased Tonnage and Other Factors of Consequence. *Proceedings, Second International Heavy Haul Railway Conference*, Association of American Railroads et al., Sept. 1982, pp. 99–117.
5. A. M. Zarembski. *Effect of Increasing Axle Loads on Rail Fatigue Life*. AAR Report R-485. Association of American Railroads, Washington, D.C., June 1981.
6. H. P. Lieurade, R. Y. Deroche, B. Deboule, and R. Conti. A Study of the Shelling Mechanism of Rails. Report RE 1302. Presented at Second International Symposium on Contact Mechanics and Wear of Rail/Wheel Systems, University of Rhode Island, Kingston, July 8–10, 1986.
7. T. G. Johns, K. B. Davies, P. M. McGuire, and S. G. Sampath. *Engineering Analysis of Stresses in Railroad Rail*. Report DOT-TSC-1038. Battelle Columbus Laboratory, June 1977.
8. A. B. Perlman, D. Y. Joeng, and O. Orringer. Rail Flaw Growth Investigations. *AREA Bulletin 688*. Vol. 83, 1982, pp. 536–550.
9. R. K. Steele. The Consequences of Truly Effective Lubrication Upon Rail Performance. ASME Paper 84-WA/RT-17. Presented at the Winter Meeting, American Society of Mechanical Engineers, New Orleans, La., 1984.
10. G. C. Schilling and G. T. Blake. *Measurement of Triaxial Residual Stresses in Railroad Rail*. AAR Report R-477. Association of American Railroads, Washington, D.C., March 1981.
11. J. J. Groom. *Final Report on Task 2: Residual Stress Determination*. Report DOT-TSC-1426. Battelle Columbus Laboratory, Nov. 1979.
12. S. G. Sampath, D. R. Albeck, J. C. Kennedy, B. N. Leis, and R. C. Rice. *Analysis of Service Stresses in Rails*. Report DOT-TSC-1663. Battelle Columbus Laboratory, Sept. 1982.
13. G. J. Fowler. *Fatigue Crack Initiation and Propagation in Pearlitic Rail Steels*. Ph.D. dissertation. School of Engineering and Applied Science, University of California, Los Angeles, 1976.
14. A. J. McEvily and K. Minakawa. *Metallurgical Evaluation of FAST Rail Steels*. Report DOT-TSC-1551. University of Connecticut, Storrs, Aug. 1981.
15. G. E. Dieter. *Mechanical Metallurgy*, 2nd ed. McGraw-Hill, New York, 1976, pp. 414–415.
16. A. D. Hearle and K. L. Johnson. Mode II Stress Intensity Factors for a Crack Parallel to the Surface of an Elastic Half-Space Subjected to a Moving Point Load. *Journal of the Mechanics and Physics of Solids*, Vol. 33, No. 1, 1985, pp. 61–81.
17. T. N. Farris, L. M. Keer, and R. K. Steele. The Effect of Service Loading on Shell Growth in Rails. *Journal of the Mechanics and Physics of Solids*, Vol. 35, No. 6, 1987, pp. 671–700.
18. T. N. Farris, L. M. Keer, and R. K. Steele. *Life Prediction for Unstable Shell Growth in Rails*. AAR Report R-655. Association of American Railroads, Washington, D.C., March 1987. (Also to be published in the *Journal of Engineering for Industry*.)
19. O. Orringer, J. M. Morris, and D. Y. Jeong. Detail Fracture Growth in Rails: Test Results. *Theoretical and Applied Fracture Mechanics*, Vol. 5, 1986, pp. 63–95.
20. P. M. Besuner. *Fracture Mechanics Analysis of Rails with Shell-Initiated Transverse Cracks*. In *Rail Steels—Developments, Processing and Use*, ASTM STP-644, American Society for Testing and Materials, Philadelphia, Pa., 1978, pp. 303–329.
21. M. J. Wisnowski. *Description of a Failed Rail from FAST*. AAR Report R-371. Association of American Railroads, Washington, D.C., Feb. 1980. (Also published as Report TTC/TM-98.)
22. J. J. Scutti. *Fatigue Properties of Rail Steel*. MS thesis. Massachusetts Institute of Technology, Cambridge, 1982.
23. R. K. Steele and D. H. Stone. Developments in Railroad Rail. *AREA Bulletin 707*, Vol. 87, 1986, pp. 311–358.
24. F. S. Hewes et al. Report on Assignment 11—Investigate the Causes of Shelly Spots and Head Checks in Rail Surfaces for the Purpose of Developing Measures for Their Prevention. *Proc. AREA*, Vol. 44, 1943, pp. 597–601.
25. F. S. Hewes et al. Report on Assignment 11—Investigate the Causes of Shelly Spots and Head Checks in Rail Surfaces for the Purpose of Developing Measures for Their Prevention. *Proc. AREA*, Vol. 45, 1944, pp. 446–462.
26. S. Kumar and S. P. Singh. *A Theoretical Study of Wheel-Rail Contact Stresses and Their Tread-Crown Curvature Relationship for Heavy Axle Loads*. Technical Report 1. Association of American Railroads, Washington, D.C., 1986.
27. H. F. Moore. Progress Report of the Joint Investigation of Fissures in Railroad Rails. *Proc. AREA*, Vol. 36, 1935, pp. 1065–1074.
28. D. D. Davis, M. J. Joerms, O. Orringer, and R. K. Steele. The Economic Consequences of Rail Integrity. *Proceedings, Third International Heavy Haul Conference*, Association of American Railroads et al., Oct. 1986.


# APPENDIX
# PHOENIX—The Model

This appendix deals with the theoretical basis of the PHOENIX model. Assumptions made by the model as well as modeling limitations will also be discussed.

## INTRODUCTION

PHOENIX is a computer simulation of rail fatigue life under various operating conditions. It takes into account such factors as rail size, wear rate, foundation modulus, and wheel size. With the current stresses calculated and those input into the model, PHOENIX predicts the initiation of internal defects within the rail head where wheel and rail contact contributes to that initiation.

PHOENIX is designed to perform parametric studies of rail fatigue behavior for diverse operating conditions. Because of the statistical nature of fatigue analysis, it is impossible to calculate absolute values for rail life, but relative comparisons of different conditions can be obtained. The model can be run on an IBM personal computer, although extensive parametric studies should be performed on a larger machine. The model is easy to use and can be customized for particular conditions without reprogramming.

## BACKGROUND

PHOENIX was designed to provide a more realistic analytical description of the rail fatigue crack initiation process than has been possible with the uniaxial model, RFLAP. The uniaxial model predicts that fatigue crack initiation should occur at the running surface of the rail, whereas rail head defects such as shells and TDs from shells, vertical split heads, and compound fractures actually initiate within the head well beneath the running surface.

The uniaxial model was made to generate believable fatigue life estimates by ignoring the short life calculations near the surface and by arbitrarily selecting a depth that is typical of shell formation. This approach is fundamentally flawed, however, because the depth of shell initiation is a function of the service history of the rail and of the inherent fatigue resistance of the rail at the region of initiation.

The underlying difficulty with the uniaxial model is that it ignores the important role of contact stresses in the transverse and vertical dimensions and that it recognizes neither the existence of a three-dimensional residual stress state nor its variation with depth and position within the rail head.

The effective stress that induces plastic flow (and leads to accumulation of fatigue initiation damage) is the octahedral shear stress; this reaches a maximum well beneath the running surface. Continuing progressive plastic flow will occur at and directly below the running surface of the rail as a result of repeated wheel passages if the wheel load exceeds some critical value (approximately 900 lb/in. of wheel diameter in the absence of externally imposed surface tractions). This plastic flow generates an internal residual stress state that is highly compressive near the surface but becomes tensile at greater depths.

Typically, shells develop in the region just at the boundary between the upper, plastically deformed, work-hardened region and the lower, undeformed base material. Therefore, the fatigue crack initiation process must respond to the combined action of varying three-dimensional stresses (both contact and flexural) and the steady stresses [residual (resulting from mill processing and service exposure), thermal, and the mean of the varying stresses]. It is this response that PHOENIX seeks to describe.

## THEORY

The operation of PHOENIX is described in three parts: how wear enters into the model, the computation and combination of the three stress systems (flexural, residual, and contact), and the prediction of crack initiation. Limitations and applications of PHOENIX are discussed last.

### Time, Tonnage, and Wear

The progress of a PHOENIX simulation is controlled by tonnage and wear rather than by time. Time does not enter into the simulation. Because wear is not presently computed internally, the wear rate appropriate for the given load must be specified by the user. Wear units are millimeters per 100 MGT. The simulation also requires a tonnage increment, which specifies how often the wear and fatigue calculations are to be made. This is normally set to 10 MGT, but can be changed. A very high wear rate would require a smaller tonnage increment, whereas a very low wear rate (well lubricated rail) could use a longer increment. If a tonnage increment is too long, loss of accuracy may result; too short an increment will only increase simulation time.

### Evaluation Points

Stress and fatigue damage are evaluated at various depths beneath the surface of the rail. In the standard configuration there are 20 points, starting at the surface and spaced 1 mm apart. These points are positioned relative to the initial rail surface (at the start of the simulation) and do not move with the current running surface. Because fatigue damage is computed only at these points, there may be some granularity in the results. If this proves to be a problem, more points may be defined (up to 40 in this implementation) or the points may be redistributed for better coverage of the depth of interest. Of course, the more points, the longer the simulation will take to run.

### Residual Stress

The triaxial residual stress field is derived from data obtained experimentally from sample rails. It is internally modelled as a cubic equation. A scale factor and a bias may be applied. The bias (or offset) may be used to simulate expansion or contraction due to temperature changes. Because strain hardening is assumed to occur much faster than wear as the current running surface recedes, the entire residual stress field moves with it. It is important to note that the residual stress calculation is very empirical and is based on a small amount of data. Residual stress fields found in rails in service can be expected to vary substantially.

### Contact Stress

Contact stresses are calculated using Hertzian contact, which implies the absence of surface tractions within the wheel-rail contact patch. Both the "crossed cylinder" and line contact configurations can be used. The crossed cylinder configuration is appropriate for a contact between a new wheel and new rail where little wear has occurred. The line contact configuration assumes that the rail head has become quite flat, making the contact patch very wide. Line contact is difficult to use because a poor choice of the contact width will cause substantial errors in the calculated contact stresses.

### Flexural Stress

Like three-dimensional residual stress and contact stresses, three-dimensional flexural stress occurs as the wheel moves

over a position on the rail. However, unlike the contact and residual stresses, only the longitudinal component of flexural stress (for vertical bending) appears to have large enough peak values to contribute to the effective stress term, $\sigma_{eff}$. Several points should be noted about the longitudinal flexural stress:

- At the running surface of the rail, it changes from mildly tensile when the wheel is approximately 5 ft away to strongly compressive when the wheel is directly over the point in question. Thus, in the head the mean stress associated with the longitudinal flexural stress is compressive.
- In addition to the overall beam-bending stress system, there is also a local HOW bending stress system in which the bottom of the rail head can be placed in tension directly under the wheel. The tendency for the HOW system to place the bottom of the head into tension is most evident when the track is stiff.

PHOENIX flexural stress calculations are based on the beam on elastic foundation (BEF) theory. A separate BEF calculation is performed for the rail head bending on the web. The two stress calculations are then superimposed to provide the total flexural stress. The present flexural stress package considers only longitudinal stresses and does not handle lateral loads.

### Effective Stress

The key to the estimation of fatigue damage under the influence of a three-dimensional stress state is the selection of a suitable damage criterion. PHOENIX utilizes the Sines criterion, which permits the calculation of an effective stress made up of both varying and steady components of principal stress. The form of the criterion is

$$\sigma_{eff} = C_1[\Sigma(\Delta\sigma_{i,j}^{amp})^2]^{1/2} + C_2\Sigma\sigma_i^{steady}$$

where

$i, j$ = principal stress; $i, j = 1 \ldots 3$, $i \neq j$;
$\Delta\sigma_{i,j}^{amp}$ = differences between the principal stress amplitudes;
$\sigma_i^{steady}$ = steady principal stresses, including the mean stresses of the varying stress ranges;
$C_1$ = fixed constant; and
$C_2$ = constant, the value of which depends on the fatigue life, which is calculated from $\sigma_{eff}$.

The term $[\Sigma(\Delta\sigma_{i,j}^{amp})^2]^{1/2}$ is directly related to the octahedral shear stress.

### Crack Initiation and Statistical Nature of Fatigue

PHOENIX determines the actual life at each of the evaluation depths by calculating the damage fraction for each load in a histogram (spectra) of loads. The tonnage increments are repeated until the damage fraction at any one depth evaluated reaches unity. At this point in tonnage and depth, fatigue crack initiation is considered to have taken place.

The damage fraction (DF) is calculated along the lines of Miner's law:

$$DF = \sum_L \frac{N}{N_f}$$

where $N$ is the number of cycles in a block of load $L$ only, and $N_f$ is the total number of cycles expected to cause fatigue crack initiation for a specified life percentile at the total stress state associated with (but not necessarily caused solely by) load $L$.

"Life percentile" refers to the fact that under the influence of fixed repetitive load (i.e., the stress history), fatigue failures do not all occur simultaneously; rather, they are spread out over a period of loading in a relatively well-behaved distribution. Thus, if one is to calculate "life," the life percentile must be specified.

In a fatigue life prediction analysis based on stress state, the value of $N_f$ can be obtained from laboratory constant stress-life tests (*S/N* tests). However, a substantial number of replicate tests must be made at each stress level in order to define the life distribution from which the life percentile is taken. Normally, if relatively few laboratory specimens are tested at each stress level, the *S/N* plot obtained is presumed to define the 50th life percentile. Typically, PHOENIX calculations are made at lst, 5th, 10th, and 20th percentiles, although this is user specified. The effects of work hardening of the running surface can also be included by specifying surface and interior hardnesses and a depth range over which the hardness transition occurs.

### Limitations and Applications

There are problems in using any fatigue model (including PHOENIX) to make exact life predictions. First, the residual stress state within any individual rail or even group of rails is entirely unknown and cannot be predicted accurately at present from a knowledge of service history. Moreover, the actual applied stress state is not really known either; this is especially the case for the contact stress because it is highly sensitive to actual wheel and rail profiles; true Hertzian contact exists only for new wheel and rail profiles. Finally, the inherent fatigue resistance character of the rail steel can be highly variable and is unknown for any individual rail or group of rails. Small variations in stress state or material fatigue resistance can yield large variations in life.

In spite of these limitations, modeling the rail fatigue crack initiation process can be informative if for no other reason than to allow an engineering estimate of best- and worst-case conditions when some important material, track, or service condition is altered. For instance, if the cleanest (freest of nonmetallic inclusions) rail steel for which *S/N* data are available or a 300-BHN standard carbon rail were compared with the derived overall rail life distribution (FAST tangent track conditions), significant improvement in fatigue life (2 to 2.5 times) would be expected. Also, the effect of rail wear on rail fatigue life can be gauged. Modest wear tends to prolong fatigue life and that effect is most pronounced at larger (more worn) crown radii and at longer life percentiles.